

# Instanton Content of the $SU(3)$ Vacuum

Anna Hasenfratz and Chet Nieter  
Department of Physics  
University of Colorado, Boulder CO 80309-390

January 2018

## Abstract

We study the topological content of the  $SU(3)$  vacuum using the renormalization group (RG) mapping method. RG mapping is a simple smoothing algorithm, in which a series of APE-smearing steps are done while the topological content of the configuration is carefully monitored. This monitoring process makes it possible to separate true topological objects from vacuum fluctuations and allows an extrapolation to zero smearing steps. Using RG mapping we have measured the instanton distribution and topological susceptibility for  $SU(3)$  gauge theory. We arrive at a value for the topological susceptibility,  $\chi^{1/4}$  of 203(5) MeV. The size distribution peaks at  $\rho = 0.3\text{fm}$ , and is in good agreement with the prediction of instanton liquid models.

# 1 Introduction

Instantons play an essential role in the QCD vacuum. In addition to explaining the U(1) problem [1, 2], there is growing evidence both from phenomenological models [3, 4] and lattice simulations [5, 6] that they play a major role in chiral symmetry breaking and the low energy hadron spectrum.

Phenomenological instanton liquid models (ILM) describe the propagation of quarks in the instanton vacuum as hopping from instanton to instanton. This "hopping propagation" can happen only if the vacuum is filled with instantons and anti-instantons that overlap and provide a continuous path for the propagation. To understand if such a path is formed one has to determine the location and size distribution of instantons in the vacuum.

Over the last few years we have developed several methods, all based on renormalization group transformations, to study the vacuum of gauge theories [7, 8, 9]. Until now we applied these methods to SU(2) gauge theories. Our results for SU(2) gauge theory indicate that while the instantons of the vacuum do not form a dense liquid, they do form some kind of percolating liquid that is sufficient for the hopping propagation [8, 9]. We also studied the role of topology by extracting the location and size of the individual instantons of the vacuum and built artificial configurations that contained only the instantons of the vacuum but none of the vacuum fluctuations or other topological objects [6]. On these smooth instanton configurations we found evidence for chiral symmetry breaking supporting the ILM picture.

This paper is the first in a series where we attempt to understand the role of instantons in the more realistic SU(3) vacuum. Here we concentrate on the properties of the instantons. By generalizing the RG mapping method we developed for the SU(2) model, we measure the topological charge and also extract the location and size of individual topological objects of the vacuum configurations. The RG mapping method is a simple and fast procedure. It is based on renormalization group methods but at the end it is only a series of APE smearing steps. What distinguishes it from other algorithms is that we carefully monitor the change of the configurations while doing as few smearing steps as possible, and extrapolate back to zero smearing. With that we can minimize the effect of the smearing procedure while use the smoothing effect to get rid of the vacuum fluctuations. We find for the topological susceptibility the value  $\chi^{1/4} = 203(5)\text{MeV}$ , in agreement with recently published calculations [10, 11, 12, 13]. However, our instanton size distribution is quite different from the published results. We find that the instanton distribution peaks at around  $\rho = 0.3\text{fm}$ . This value is significantly smaller than those of Ref. [10, 11] but in excellent agreement with the ILM predictions [14]. Our results for the density

of the instantons in the vacuum is also in agreement with phenomenological expectations. We found the density to be about  $1.1\text{fm}^{-4}$ .

The rest of this paper is organized as follows. In Chapter 2 we will discuss the RG mapping method and demonstrate why it is necessary to monitor the instantons during the smearing procedure. Chapter 3 is our results for the topological susceptibility and instanton size distribution. Chapter 4 is the summary.

## 2 RG mapping

Instantons carry only a few percent of the total action of typical Monte Carlo configurations - they are hidden by the vacuum fluctuations. The goal of any method designed to reveal the vacuum structure is to reduce the short range quantum fluctuations in the gauge fields while preserving the topological content of the vacuum.

The method of inverse blocking [15, 16, 7] is one of the theoretically best supported smoothing algorithms. For any coarse lattice the inverse block transformation finds the smoothest lattice with half the lattice spacing and twice the lattice size that blocks back into the original lattice, and consequently has the same topological structure as the original lattice. In Ref. [7] we have used the inverse blocking method to calculate the topological susceptibility of the  $SU(2)$  vacuum. Unfortunately inverse blocking requires an extensive amount of computer resources and cannot be used repeatedly due to rapidly increasing memory requirements. Therefore we could not use inverse blocking to measure the instanton size distribution of the vacuum or do a reliable scaling test for the susceptibility by going to smaller lattice spacing and larger lattices.

The method of RG cycling [8] combines the inverse blocking with an additional blocking step that makes it possible to apply it repeatedly until the gauge configuration becomes sufficiently smooth. That way it is possible to reveal the instanton size distribution of the vacuum, but because RG cycling still contains an inverse blocking step, it is also computer intensive and cannot be used on large lattices.

Our next method, RG mapping, was designed to mimic the inverse-blocking-blocking sequence of the RG cycling without actually performing the inverse blocking step. In Ref. [9] the RG cycling transformation for  $SU(2)$  was fitted to a simple transformation where each link is replaced by an APE-smear link

[17]

$$\begin{aligned}
X_\mu(x) = (1 - c)U_\mu(x) &+ c/6 \sum_{\nu \neq \mu} (U_\nu(x)U_\mu(x + \hat{\nu})U_\mu(x + \hat{\nu})^\dagger \\
&+ U_\nu(x - \hat{\nu})^\dagger U_\mu(x - \hat{\nu})U_\mu(x - \hat{\nu} + \hat{\mu})), \quad (1)
\end{aligned}$$

with  $X_\mu(x)$  projected back onto  $SU(2)$ . The best fit between a RG cycled lattice and a smeared lattice was obtained by choosing  $c = 0.45$  and performing two smearing steps. This transformation reduces the short range fluctuations effectively and reproduces the result of RG cycling at least for instantons that are larger than about 1.5 lattice spacing, yet the computer resources that it uses are insignificant compared to those required for RG cycling.

While for  $SU(2)$  we adjusted the parameters of the RG mapping method to match one RG cycling step, the exact correspondence is really not necessary as long as the evolution of the configuration is monitored. Nevertheless we decided to use the same smearing parameter  $c = 0.45$  for the present  $SU(3)$  study. We found that with that choice 15-30 smearing steps were necessary to reveal the vacuum structure of the configurations.

## 2.1 The effect of RG mapping on instantons

During RG mapping, just like during RG cycling, the charge density profile (i.e. instanton size) changes slowly and usually monotonically. Over several smearing steps these changes can be significant requiring a careful monitoring of the configuration as it is smoothed. Since we are interested in the topological content of the original and not the smoothed configurations, an extrapolation to zero smoothing steps must be done. Fortunately the location of the instantons are fairly stable and monitoring of the instantons can be done straightforwardly.

Figure 1 illustrates how typical instantons change during the smearing procedure. This  $\beta = 6.0$ ,  $16^4$  configuration has a total charge of  $Q = 4$ . We followed the evolution of the instantons between 6 and 24 smearings with smearing parameter  $c = 0.45$ , and then again between 40 and 48 steps, to study their behavior after a large number of smearing steps. A total of five stable objects were found on this configuration, four instantons and one anti-instanton. The location of each of the identified objects was stable, it changed by no more than one lattice units in any of the coordinates of the lattice. Figure 1 shows the sizes of these objects as the configuration is smeared. The solid lines are linear extrapolations based on smearing steps 16 to 24. The slopes of all the extrapolations are less than 0.03, except for the anti-instanton, which changes more rapidly. The linear extrapolations match the evolution out to large smearing

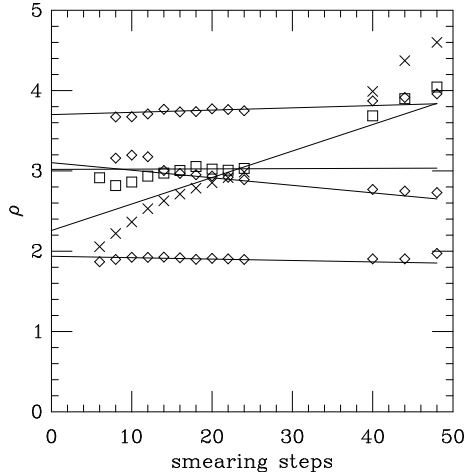


Figure 1: Radius versus APE-smearing steps of instantons (for clarity, two symbols, diamonds and squares both denote instantons) and anti-instantons (crosses) on a  $16^4$   $\beta = 6.0$  configuration.

steps for three out of the five objects. Since the total charge on this configuration is  $Q = 4$ , the instanton finding algorithm either missed an instanton or the anti-instanton is not there, it is only a miss-identified vacuum fluctuation. The latter option is supported by the fact that the anti-instanton changes more rapidly than the instantons of the configuration.

### 3 Results

#### 3.1 Parameters of the Simulation

We have used Wilson action at couplings  $\beta = 5.85, 6.0$  and  $6.1$ . The parameters of the simulations are given in Table 1. The configurations were separated by 150 sweeps and all of the lattices are periodic. The lattice spacings in Table 1 were calculated using the results for the  $r_0$  parameter and the parametrization of the string tension of Ref. [18]. Since the string tension in [18] is set at  $\sqrt{\sigma} = 465\text{MeV}$ , about 5% higher than the customary  $\sqrt{\sigma} = 440\text{MeV}$  value, our lattice spacings are somewhat smaller than in other works.

Table 1: Parameters of the simulations

$\beta$	L	number of configurations	a [fm]	La [fm]
5.85	12	150	0.121(1)	1.46
6.0	12	426	0.093(1)	1.12
6.0	16	100	0.093(1)	1.49
6.1	16	212	0.079(1)	1.27

### 3.2 The Topological Susceptibility

We have used the FP algebraic operator developed for SU(2) in [8] to measure the topological charge. The operator usually gave an integer value within a few percent after 12 APE smearing steps and remained stable during the smoothing process. Occasionally it started to change rapidly settling at a different integer value after a few smearing steps. This change describes the disappearance of an instanton from the lattice. We have seen that phenomena in SU(2) as well. The charge for SU(3) was generally more stable under smoothing than for SU(2). This is probably due to the suppression of very small instantons in SU(3) as we will discuss in the next section.

We have monitored the change of the topological charge under smoothing carefully. The charge was measured every two APE steps for each configuration between smoothing steps 12 and 24 for the  $\beta = 5.85$  and the  $12^4$   $\beta = 6.0$  configurations, between 16 and 28 steps for the  $16^4$   $\beta = 6.0$  configurations, and 20 and 32 steps for the  $\beta = 6.1$  configurations. Fig. 2 shows the average value of the charge squared  $\langle Q^2 \rangle$  versus the number of smearing steps. Since the susceptibility is stable, there is no reason to extrapolate back to zero smearing steps. Table 2 contains the results for  $\langle Q^2 \rangle$  and  $\chi^{1/4}$ . The given errors in  $\chi^{1/4}$  are due to the statistical error of  $\langle Q^2 \rangle$ . The errors due to the uncertainty in the lattice spacing are negligible.

The susceptibility increases by about 5% from  $\beta = 5.85$  to  $\beta = 6.0$  but stabilizes at higher values of  $\beta$ . This difference can be attributed to the lack of small instantons at  $\beta = 5.85$  due to the larger lattice spacing. The  $\beta = 6.0$ ,  $12^4$  lattices likely show a small finite volume effect. We arrive at a value for the  $\chi^{1/4}$  of 203(5)MeV. Before we compare our results with those from other work, we should first note the string tension value we used is higher than the standard value by about 5%. Had we used the customary  $\sqrt{\sigma} = 440$ MeV value, we'd obtained  $\chi^{1/4} = 192(5)$ MeV, in complete agreement with the results from Ref. [10, 11, 12].

Table 2: Results for the susceptibility

$\beta$	L	smearing	$\langle Q^2 \rangle$	$\chi^{1/4}[\text{MeV}]$
5.85	12	16	4.1(4)	192(5)
		20	4.0(4)	191(5)
		24	4.0(4)	191(5)
6.0	12	16	1.6(1)	198(3)
		20	1.6(1)	198(3)
		24	1.6(1)	198(3)
	16	16	5.6(8)	203(7)
		20	5.6(8)	203(7)
		24	5.6(8)	203(7)
6.1	16	20	2.9(3)	203(5)
		26	2.9(3)	203(5)
		32	2.9(3)	203(5)

### 3.3 The Instanton Size Distribution

We have identified instantons every 2 APE-smearing steps between 16 and 32 smearing steps with parameter  $c=0.45$ . The identification of the instantons and the measurement of their sizes was done in the same manner as in Ref. [8], and the instanton sizes were extrapolated back to zero smearing steps. The reason for monitoring instantons is twofold. First, instantons change, usually grow during the smearing process, as we illustrated in Sect. 2.1. The other reason is that monitoring helps distinguish true topological objects from vacuum fluctuations. In Figure 3, we plot the size distribution of instantons after 12 and 24 smearing steps at  $\beta = 6.0$ . The peak of the distribution changes from 0.34fm to 0.40fm as we perform the additional 12 smearing steps and the shape of the distribution also changes. The number of objects found decreases by about 50%, and distribution develops a tail at larger  $\rho$  values. The development of the tail in the distribution is consistent with the observation that the size of the instantons grow with the smearing steps. The decrease in the number of objects signals that on the 12 times smeared lattice we identified many fluctuations as topological objects. In fact, even after 24 smearing steps the instantons density is still  $2.9\text{fm}^4$ , close to three times larger than the phenomenologically expected value. That indicates that even after 24 smearing steps we still have a lot of "spurious instantons". To counter this we only identify an object as an instanton or anti-instanton if it appears to be stable over several smearing steps. To call an object stable we require not only that its location is stable during smoothing but also that its size does not change too fast. We approximate the change of the size linearly and if the slope of the linear fit is above some cut-off, the object is rejected. We choose this cut-off value so that the charge calculated by

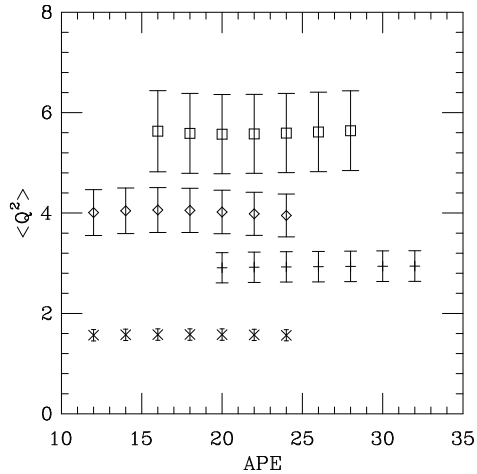


Figure 2: The susceptibility  $\langle Q^2 \rangle$  vs number of  $c = 0.45$  APE steps. Symbols are diamonds for  $\beta = 5.85$ , crosses for  $\beta = 6.0$  on  $12^4$  lattices, squares for  $\beta = 6.0$  on  $16^4$  lattices, and pluses for  $\beta = 6.1$ .

taking the difference between the total number of instantons and anti-instantons found on the configurations give the same topological susceptibility as the charge measured directly with the FP operator  $\langle Q = (I - A)^2 \rangle = \langle Q_{FP}^2 \rangle$ .

On the  $12^4$  lattices at  $\beta = 6.0$  a cut-off 0.035 per smearing steps gave identical susceptibility with the two methods and predicted the density of instantons to be 1.1 per  $\text{fm}^4$ . The results on the other configurations were consistent with that but the error of  $\langle Q = (I - A)^2 \rangle$  were too large to get a precise determination of the cut. However, the instanton density is much better measured, and we found that a cut of 0.035 gave consistently 1.1 per  $\text{fm}^4$  density. Since the same cut-off value was found for SU(2) as well, in our analysis we used a cut-off 0.035, i.e. we kept only those instantons whose size in lattice units changed not faster than 0.035 per smearing step.

In their recent work Smith and Teper [11] also used APE smearing to smooth the configurations. They chose a smearing parameter  $c=0.86$ , almost twice of ours and smoothed the configurations 23 to 46 times. We do not have much experience about how the larger  $c$  parameter effects the instantons of the lattice. As a rough estimate one can consider the product  $\sqrt{N_s c}$ , where  $N_s$  denotes the number of smearing steps, as a characteristic number of the amount of smearing. Using that quantity, Ref. [11] has 3-4 times more smearing than this calculation. Figure 9. of [11] is a similar plot to our Figure 3, showing the size



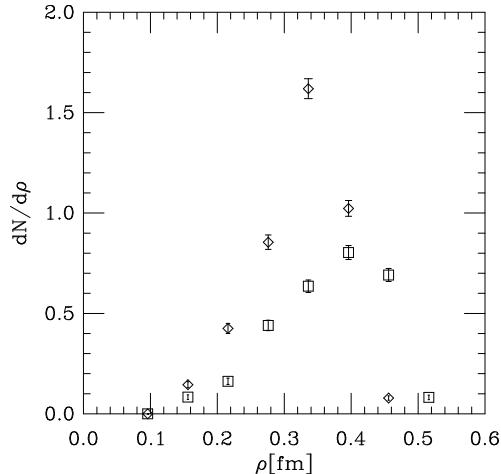


Figure 3: The size distribution on 12 (diamonds) and 24 (squares) times smeared  $12^4$  lattices at  $\beta = 6.0$ .

distribution at  $\beta = 6.0$  after 23, 28, 32 and 46 smoothing steps with  $c=0.86$  APE parameter. There the change due to smearing is less pronounced than in our case, as the average instanton size changes from 0.49fm to 0.53fm. It is difficult to compare our numbers directly to those of Ref. [11] since we used a different smearing parameter and we did not do the fine tuned filtering of [11] at this level. Nevertheless, it is clear that smoothing effects the instanton size distribution and it is not surprising that in Ref. [11] the observed distribution peaks at a larger  $\rho$  value. Our goal is to correct for the change in instanton size by extrapolating the results back to zero smearing steps.

Our final result for the instanton size distribution after extrapolation is shown in Figure 4. We overlay the data obtained at  $\beta = 5.85$  (diamonds),  $\beta = 6.0$  (octagons), and  $\beta = 6.1$  (squares). The data points for  $\beta = 6.0$  is a combination of the results from both lattice sizes. The bin size is 0.06 fm and the distribution  $dN/d\rho$  is measured in  $\text{fm}^4$ . The second bin of each distribution starts at  $\rho = 1.6a$ . Because smearing cannot identify instantons below a certain size, the first bin in each distribution is unreliable.

The solid line is a fit to a two loop perturbative instanton distribution formula with a “regularized” log [14]

$$S_I = \frac{8\pi^2}{g^2(\rho)} = b_0 L + b_1 \log L,$$

$$L = \frac{1}{p} \log[(\rho \Lambda_{inst})^{-p} + C^p], \quad (2)$$

where  $b_0 = \frac{11}{3}N_c$ ,  $b_1 = \frac{17}{11}N_c$ , and  $p$  and  $C$  are arbitrary parameters. One would expect Eqn. 2 to be valid if the instanton size distribution is regulated by quantum fluctuations. Our fit corresponds to  $p = 5.5$ ,  $C = 5.5$  and  $\Lambda_{inst} = 0.71 \text{ fm}^{-1}$ . This  $\Lambda_{inst}$  corresponds to  $\Lambda_{\bar{M}\bar{S}} = 1.45\Lambda_{inst} = 206 \text{ MeV}$ , considerably smaller than the value  $\Lambda_{\bar{M}\bar{S}} = 270 \text{ MeV}$  obtained from recent string tension data. The implication of this discrepancy, if any, is not clear. After all, Eqn. 2 is only a phenomenological form, even if the instanton size distribution is regulated by quantum fluctuations, there is no proof that the logarithms should be regularized this way.

The main difference between the SU(3) distribution and the one we found for SU(2) [8, 9] is the lack of small instantons. For small instantons the instanton distribution can be described by the semiclassical dilute instanton model which predicts that  $\frac{dN}{d\rho} \sim \rho^{b_0}$ , therefore small instantons are indeed suppressed in SU(3) relative to SU(2). That explains why the topological charge and the topological susceptibility are more stable under smoothing in SU(3).

The three different coupling values predict a consistent size distribution indicating scaling. The size distribution peaks at around  $\bar{\rho} = 0.3 \text{ fm}$ . This value is considerably smaller than the results of Ref. [10]. who found  $\rho_{peak} = 0.6 \text{ fm}$  or the result of Ref. [11] who quote  $\bar{\rho} = 0.5 \text{ fm}$ . The difference between our result and [11] is most likely due to our extrapolation to zero smearing step. Ref. [10] uses improved cooling as a smoothing method. We do not have direct comparison of the techniques. It would be interesting to monitor individual instantons under cooling and see if and how their sizes change. The phenomenological instanton liquid model predicts  $\rho_{peak} = 0.28 - 0.33 \text{ fm}$ , depending on the  $\Lambda$  parameter used in the calculation [4, 14]. That value is consistent with our result.

## 4 Summary

Using the RG mapping method we calculated the topological susceptibility and the instanton size distribution for SU(3) gauge theory. This technique, developed originally for the SU(2) gauge model and based on different renormalization group methods, is a fast and simple smoothing algorithm. It consists of several APE smearing steps. What distinguishes it from similar methods is that only the minimal number of smearing steps are performed and the topological content of the configuration is continuously monitored. That makes it possible to

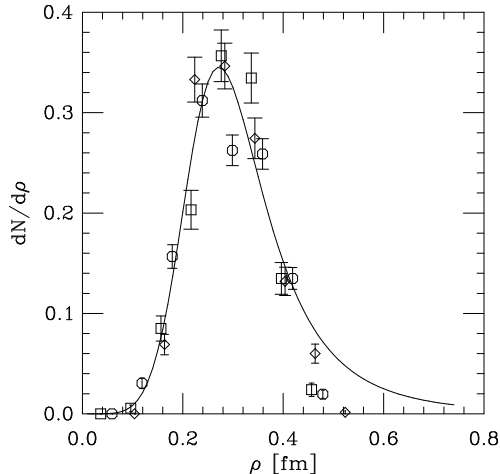


Figure 4: The size distribution of the instantons. The diamonds correspond to  $\beta = 5.85$ , octagons to  $\beta = 6.0$ , and squares to  $\beta = 6.1$ . The first bin of each distribution is contaminated by the cut-off. The solid curve is a three parameter fit to the

separate vacuum fluctuations from true topological objects and to control the change in size of the instantons during the smearing process.

We found scaling for both the topological susceptibility and the instanton size distribution in the lattice spacing range of 0.12fm to 0.079fm. Our value for the topological susceptibility,  $\chi^{1/4} = 203(5)\text{MeV}$  is consistent with other recent calculation but our instanton size distribution predicts considerably smaller instantons. We attribute this discrepancy to the change of the size of topological objects, which we carefully monitor and remove. Our result for the instanton size distribution is consistent with the phenomenologically successful instanton liquid model prediction.

## Acknowledgements

We would like to thank T. DeGrand and T. Kovács for useful conversations, and E. Shuryak for clarifying many questions regarding the instanton liquid model. We would like to thank the Colorado High Energy experimental groups for allowing us to use their work stations. This work was supported by the U.S. Department of Energy grant DE-FG03-95ER-40894.

## References

- [1] S. Weinberg, Phys. Rev. D11 (1975) 3583; G. t'Hooft, Phys. Rev. D14 (1976) 3432; Phys. Rev. Lett. 37 (1976) 8.
- [2] E. Witten, Nucl. Phys. B156 (1979) 269; G. Veneziano, Nucl. Phys. B159 (1979) 213.
- [3] D. Diakanov, Lectures at the Enrico Fermi School in Physics, Varenna, 1995, hep-ph/9602375.
- [4] T. Schäfer and E. V. Shuryak, Rev. Mod. Phys. 70, (1998) 323.
- [5] T. L. Ivanenko, J W. Negele, Nucl. Phys. Proc. Suppl. 63 (1998), 504;
- [6] T. DeGrand, A. Hasenfratz, T. Kovács, Phys. Lett. B420 (1998), 97;
- [7] T. DeGrand, A. Hasenfratz, D. Zhu, Nucl. Phys. B478 (1996) 349.
- [8] T. DeGrand, A. Hasenfratz, T. Kovács, Nucl. Phys. B505 (1997) 417.
- [9] T. DeGrand, A. Hasenfratz, T. Kovács, Revealing Topological Structure in the SU(2) Vacuum, preprint COLO-HEP-393 and hep-lat/9711032.
- [10] Ph. de Forcrand, M. Garcia Perez, James Hetrick and I.-O. Stamatescu, Nucl. Phys. Proc. Suppl. 63 (1998) 406; Ph. de Forcrand, M. Garcia Perez, James Hetrick and I.-O. Stamatescu, hep-lat/9802017.
- [11] Douglas Smith and Micheal Teper, hep-lat/9801008.
- [12] R. G. Edwards, U. M. Heller, R. Narayanan, Spectral flow, chiral condensate and topology in the lattice, hep-lat/9802016.
- [13] B. Alles, M. D'Elia, and A. Di Giacomo, Nucl. Phys. B494 (1997) 281.
- [14] E. V. Shuryak, Phys. Rev. D52 (1995) 5730;
- [15] M. Blatter, R. Burkhalter, P. Hasenfratz and F. Niedermayer, Nucl. Phys. **B** (Proc. Suppl.) 42 (1995) 799; M. Blatter, R. Burkhalter, P. Hasenfratz and F. Niedermayer, Phys. Rev. D53 (1996) 923. R. Burkhalter, Phys. Rev. D54 (1996) 4121.
- [16] T. DeGrand, A. Hasenfratz, D. Zhu, Nucl. Phys., B475 (1996) 321.
- [17] M. Falcioni, M. Paciello, G. Parisi, B. Taglienti, Nucl. Phys. B251[FS13] (1985) 624. M. Albanese, et al. Phys. Lett. B192 (1987) 163.
- [18] R.G. Edwards, U. Heller, and T.R. Klassen, Accurate Scale Determinations for the Wilson Gauge Action, preprint hep-lat/971003.